Whisker alignment of Ti–6Al–4V/TiB composites during deformation by transformation superplasticity

C. Schuh, D.C. Dunand *

Department of Materials Science and Engineering, Northwestern University, MLSB 2036, 2225 N. Campus Drive, Evanston, IL 60208-3108, USA

Abstract

We examine the effect of 10 vol.% TiB whisker reinforcement on transformation superplasticity of Ti–6Al–4V, induced by thermal cycling about the α/β phase transformation range of the matrix under a uniaxial tensile stress. During superplastic deformation, the whiskers gradually align along the external loading axis, as measured by electron back-scattering diffraction of deformed specimens. The composites exhibit a gradual decrease in effective deformation rate during superplastic elongation. This effect is attributed to increased load transfer from matrix to whisker upon whisker alignment, and is explained with elastic calculations of stress partitioning. © 2001 Elsevier Science Ltd. All rights reserved.

Keywords: Superplasticity; A. Phase transformation; Titanium composites

1. Introduction

The addition of reinforcing ceramic particulates to titanium or titanium alloys results in metal matrix composites with improved strength, stiffness and abrasion resistance (Lederich et al., 1994; Ranganath, 1997). Titanium monoboride (TiB) is attractive because of its high hardness and stiffness, its low density and its chemical stability with titanium-based matrices (Saito et al., 1995). Furthermore, during powder-metallurgy processing, TiB reinforcement can be synthesized in situ within the titanium alloy matrix by the dissolution of TiB_2 particles and subsequent re-precipitation of TiB, an orthorhombic phase with whisker morphology (Saito et al.,

* Corresponding author. Tel.: +1-847-491-5370; fax: +1-847-467-6573.
E-mail address: dunand@northwestern.edu (D.C. Dunand).

1994, 1995; Saito, 1995; Funami et al., 1997). Similar microstructures can also be developed by rapid solidification processing of boron-containing titanium alloys (Fan et al., 1994; Lederich et al., 1994; Ranganath, 1997; Gorsse et al., 1998)

Since the addition of TiB reinforcement to titanium alloys reduces ductility and toughness (Abkowitz et al., 1993a; Lederich et al., 1994), traditional room-temperature forming techniques such as rolling, drawing, bending, stamping and machining are limited. High temperature processes such as forging are also much more difficult than for the unreinforced titanium alloy, while microstructural superplasticity, which relies on grain boundary sliding, can be ruled out due to the matrix grain size and non-equiaxed reinforcement and grain morphology.

Alternatively, polymorphic materials can be superplastically deformed by thermally cycling about their phase transformation range under the action of an externally-applied stress, independently of their grain size [for a recent review see Dunand (1997)]. Internal transformation-mismatch stresses are biased by the external stress, and for uniaxial deformation the strain increment $\Delta\epsilon$ produced on a complete thermal cycle is proportional to the applied stress σ. Repeated thermal cycling allows for the accumulation of superplastic strains ($>100\%$ in tension). This effect has been the subject of several recent theoretical investigations (Leblond, 1989; Leblond et al., 1989; Cherakaoui et al., 1998), and experimental studies of transformation superplasticity have demonstrated the effect for titanium (Greenwood and Johnson, 1965; Chaix and Lasalmonie, 1981; Takayama et al., 1985; Dunand and Bedell, 1996), Ti–6Al–4V (Sato et al., 1994; Schuh et al., 1999), and composites of these materials containing equiaxed TiC particles in which the matrix transformation is used to drive deformation (Dunand and Bedell, 1996; Dunand and Myojin, 1997; Schuh et al., 1999). However, no report exists on transformation superplasticity of whisker-reinforced composites. An additional issue with these composites is the alignment of the reinforcement in the matrix, which can often lead to strength and stiffness enhancements in the direction of alignment. Whisker alignment is typically accomplished by extrusion (Wu, 1979; Farkash and Brandon, 1994), or, as for polymer-matrix composites, by application of shear forces to a suspension (Folgar and Tucker, 1984).

In the present article, we report transformation superplasticity of Ti–6Al–4V reinforced with 10 vol.% TiB whiskers by confirming the linear relationship between superplastic strain increment and applied stress, and by demonstrating tensile engineering strains in excess of 100%. We further examine TiB whisker alignment during uniaxial superplastic elongation of the composites. Finally, since the biasing stress on the matrix is affected by such whisker alignment, the deformation properties are directly correlated to the degree of alignment, an effect which is modeled by considering elastic load transfer between the superplastic matrix and the aligning whiskers.

2. Experimental

Specimens of Ti–6Al–4V reinforced with 10 vol.% TiB whiskers as well as unreinforced Ti–6Al–4V were supplied by Dynamet Technology (Burlington, MA),

manufactured by their CHIP process (Abkowitz and Weihrauch, 1989; Abkowitz et al., 1993ab), which consists of elemental powder blending, cold isostatic pressing, vacuum sintering, and containerless hot-isostatic pressing (HIPing). Titanium monoboride whiskers are produced in-situ by the addition of 5 vol.% titanium diboride powders during the blending stage, which subsequently dissolve and re-precipitate as TiB whiskers during the sintering and HIPing stages (Lederich et al., 1994; Funami et al., 1997; Yamamoto et al., 1997). Cylindrical creep specimens with gauge length 20 mm and diameter 5 mm were machined from the processed billets.

Transformation superplasticity experiments were conducted in a custom-built test frame described elsewhere (Zwigl and Dunand, 1998) under a purified argon atmosphere. Rapid radiant heating with closed-loop control was employed to produce 8-minute triangular cycles between 840 and 1030°C. The controlling type-K thermocouple was positioned at the specimen gauge surface, and a second thermocouple was positioned at the specimen head. One specimen each of Ti–6Al–4V and Ti–6Al–4V/TiB was used to determine the stress dependence of the cycling strain increments $\Delta\epsilon$, measured with an LVDT at the cold end of the load train. Stable values of $\Delta\epsilon$ were typically reached after about 6–8 cycles, after which the external stress was increased. A second composite specimen was deformed to 100% engineering strain with $\sigma = 2.5$ MPa before being tested in uniaxial tension at room temperature. Finally, a series of three composite specimens were deformed with $\sigma = 2.5$ MPa to respective engineering strains of 20.1 and 46.8%, and failure at 260% for analysis of microstructural evolution during superplastic deformation. For comparison, an unreinforced specimen of Ti–6Al–4V was also deformed to failure with $\sigma = 2.5$ MPa. In each experiment, constant true stress was maintained to within 7% by manual adjustment of the applied load, assuming constant volume of the gauge section. The density of the as-received material was determined by the Archimedes method in distilled water.

Metallographic preparation consisted of grinding on SiC papers and polishing with diamond paste of 30, 6, 1, and 0.05 microns, followed by immersion etching in Kroll's reagent. Texture data of both the matrix and reinforcing whiskers of Ti–6Al–4V/TiB specimens were obtained from electron back-scattering diffraction (EBSD) patterns obtained in a field emission scanning electron microscope at TexSEM, Inc. (Draper, UT). The accelerating voltage and specimen current were 20 kV and 1.0 nA, respectively, and about 20,000 patterns were acquired over an area of approximately 80,000 μm^2 for each sample analyzed. Between 148 and 495 individual TiB whiskers were identified on a given specimen.

3. Results

3.1. As-received materials

Photomicrographs of the composite material in the as-received condition are shown in Fig. 1(a) and (b). The unetched micrograph [Fig. 1(a)] reveals a fairly
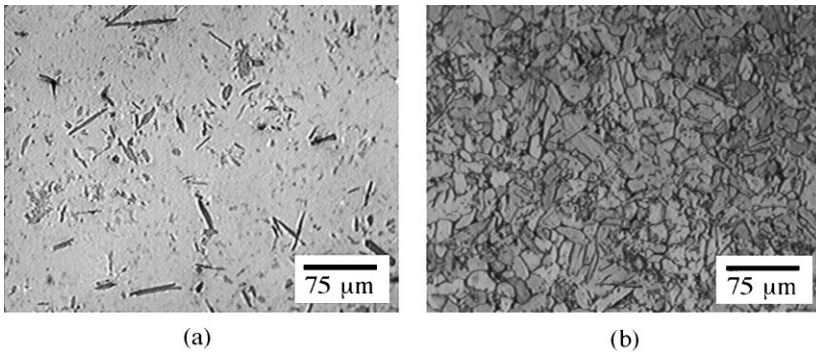
Fig. 1. Photomicrographs of as-received Ti–6Al–4V/TiB material (a) unetched and (b) etched in Kroll's reagent.

uniform distribution of randomly-oriented TiB whiskers with length of about 25–60 μm and aspect ratio of about 15–25. The homogeneity of the reinforcement distribution is reflective of the in-situ dissolution/reprecipitation which occurred during sintering, in which diffusion and allotropic transformation produced chemical and microstructural homogeneity on a fine scale. Etching [Fig. 1(b)] exposed a matrix grain structure with an average grain diameter of 15–20 μm, smaller than in the unreinforced Ti–6Al–4V alloy, for which a matrix of large β grains (∼150–250 μm diameter) and superimposed α-laths (∼75–150 μm long) was observed. This type of microstructure is commonly observed upon slow cooling of Ti–6Al–4V from above the β-transus (Anon., 1979). Because of the large and non-equiaxed microstructural dimensions of both of these materials, microstructural superplasticity by grain boundary sliding is not expected. Finally, both unreinforced Ti–6Al–4V and the Ti–6Al–4V/TiB composite were found to be fully dense (99.8% theoretical for both materials) in the as-received condition.

3.2. Transformation superplasticity of Ti–6Al–4V and Ti–6Al–4V/TiB

Fig. 2 shows for both materials the true strain increment, $\Delta\epsilon$, accumulated after each thermal cycle as a function of the uniaxial biasing stress σ. The linear relationship between these parameters indicates that the materials experienced, on average, Newtonian flow, since the average strain rate is equal to $\Delta\epsilon$ divided by the cycle time. Thus, a large resistance to plastic instabilities such as cavitation and necking is expected. The superplastic slope, $\Delta\varepsilon/\sigma$, of the composite is found to be about 0.97 GPa^{-1}, less than one-third of that for Ti–6Al–4V, 3.11 GPa^{-1}. We note that the data for the composite in Fig. 2 was acquired at total engineering strains below 15%, minimizing any effects of whisker reorientation as discussed in the following sections. For each material, the crossed data point in Fig. 2 represents a specimen separate from that of the other data points, with variations arising due to different experimental sources of error, including small differences in specimen composition, thermal conditions, etc.
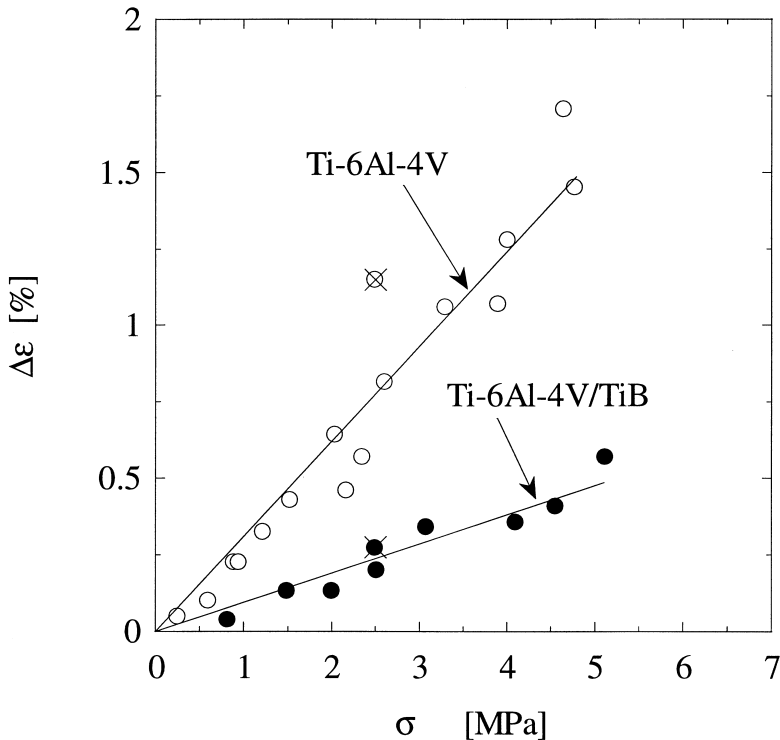
Fig. 2. Strain increment $\Delta\epsilon$ accumulated on each thermal cycle as a function of the uniaxial tensile stress σ for the Ti–6Al–4V/TiB composite and for unreinforced Ti–6Al–4V. Crossed data points are from separate specimens which correspond to the data in Fig. 4.

A photograph of the composite specimen deformed to failure with true stress $\sigma = 2.5$ MPa is shown in Fig. 3, with an engineering failure strain of 260% after 635 cycles. This can be compared with the unreinforced Ti–6Al–4V, which achieved a failure strain of 398% after only 135 cycles under the same cycling and stress conditions.

Fig. 4 shows the strain-increment history of the two specimens deformed to failure with $\sigma = 2.5$ MPa. In order to eliminate the effects of small stress variations (less than about 7% with respect to the target value of 2.5 MPa) due to load and specimen cross-section changes during the experiment, each strain increment is normalized by the instantaneous true applied stress to obtain the value of $\Delta\varepsilon/\sigma$ for each cycle, which is expected to be constant (Fig. 2). For ease of comparison, the cycle number, N, is normalized by the total number of cycles to failure, N_t. A few erratic data points associated with manual adjustments of the applied load (necessary to maintain a constant true stress) have been removed in Fig. 4. Fig. 4(a) shows that the strain increment of Ti–6Al–4V was approximately constant for most of its deformation history, followed by a period of rapid increase associated with necking and/or cavitation prior to failure. From the beginning of the test until the onset of
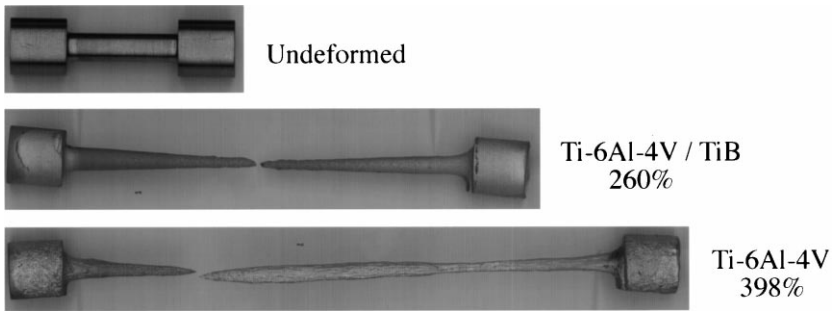
Fig. 3. Photograph of deformed composite specimen with engineering failure strain of 260% after 135 thermal cycles. Undeformed geometry and failed Ti–6Al–4V specimen are shown for comparison.
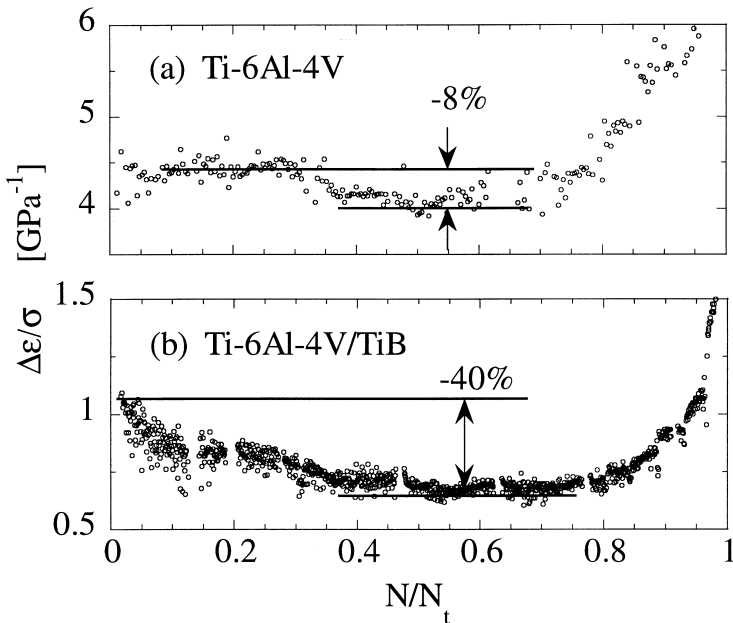

Fig. 4. Stress-normalized strain increment ($\Delta\epsilon/\sigma$) history of specimens deformed to failure: (a) unreinforced Ti–6Al–4V and (b) Ti–6Al–4V/TiB composite. N/N_t is the lifetime fraction of each specimen.

the final strain increment rise (similar to a creep tertiary stage), the maximum variation in the strain increment is about 8%. In contrast, the TiB-reinforced composite [Fig. 4(b)] experienced a significant reduction of the superplastic strain increment over the course of the experiment, about 40% from the initial value of about 1.1 GPa^{-1}. Because of this steady decrease, a true steady-state in the superplastic strain increment was not achieved. Furthermore, a smaller fraction of the composite lifetime was spent in the tertiary deformation stage.

3.3. Evolution of microstructure during superplastic deformation

The optical micrograph in Fig. 5 shows a longitudinal section of the Ti–6Al–4V/ TiB composite deformed to failure at 260% engineering strain. Comparing with Fig. 1, the alignment of the TiB whiskers along the tensile axis (horizontal in Fig. 5) after deformation is noteworthy.

EBSD was used to identify the crystallographic orientation of the orthorhombic TiB phase in each of the four specimens deformed to engineering strains of 0 (Fig. 1), 20.1, 46.8, and 260% (Fig. 5). Upon precipitation of TiB from the Ti-rich matrix during the sintering and HIPing stages of composite manufacture, growth of TiB occurs preferentially along the orthorhombic [010] direction (Hyman et al., 1989; Li et al., 1993), resulting in the formation of whiskers with their longitudinal axes parallel to TiB-[010]. Thus, a standard texture analysis of TiB on a composite cross-section of known orientation allows for the identification of the whisker orientation with respect to macroscopic specimen dimensions.

We define the axial angle, ϕ, as the angle between the longitudinal dimension of the whisker (i.e. the TiB orthorhombic [010] direction) and the tensile axis. Then the angular orientation distribution, $P(\phi)$, is a probability density distribution subject to the normalization condition:

$$\int_0^{\pi/2} P(\phi) \cdot d\phi = 1 \tag{1}$$

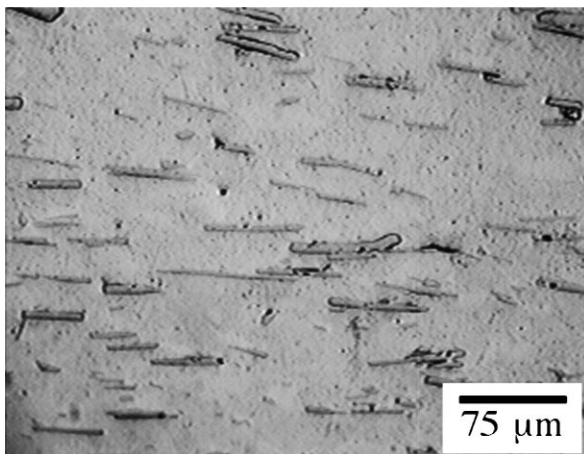as well as two symmetry conditions:

$$P(\phi + \pi) = P(\phi) \tag{2a}$$

Fig. 5. Optical micrograph of the composite deformed to failure with $\sigma = 2.5$ MPa. Tensile axis is horizontal.

$$P(-\phi) = P(\phi) \tag{2b}$$

The probability of a randomly selected whisker exhibiting axial angle between ϕ and $\phi + \delta\phi$ is the integral of $P(\phi)$ with respect to ϕ over the given interval. From the EBSD results, the axial angle of each whisker was measured with an accuracy determined primarily by the sectioning procedure. We conservatively estimate this error as less than 5° based on visual observations after the sectioning procedure. Because EBSD determines texture on a surface, and not through the volume, a simple correction as described in the Appendix allows for calculation of the true distribution $P(\phi)$ representative of the entire specimen volume.

The distribution $P(\phi)$ determined from the experimental EBSD data with the correction discussed in the Appendix is shown in Fig. 6 for an as-received specimen as well as those deformed to engineering strains of 20.1, 46.8, and 260% (failure), corresponding to 0, 100, 200, and 625 thermal cycles, respectively. The tendency for whisker alignment with deformation is striking, with a pronounced TiB texture appearing after only 20.1% engineering strain. The expected shape of $P(\phi)$ for a truly three-dimensionally random distribution of whiskers is discussed in the

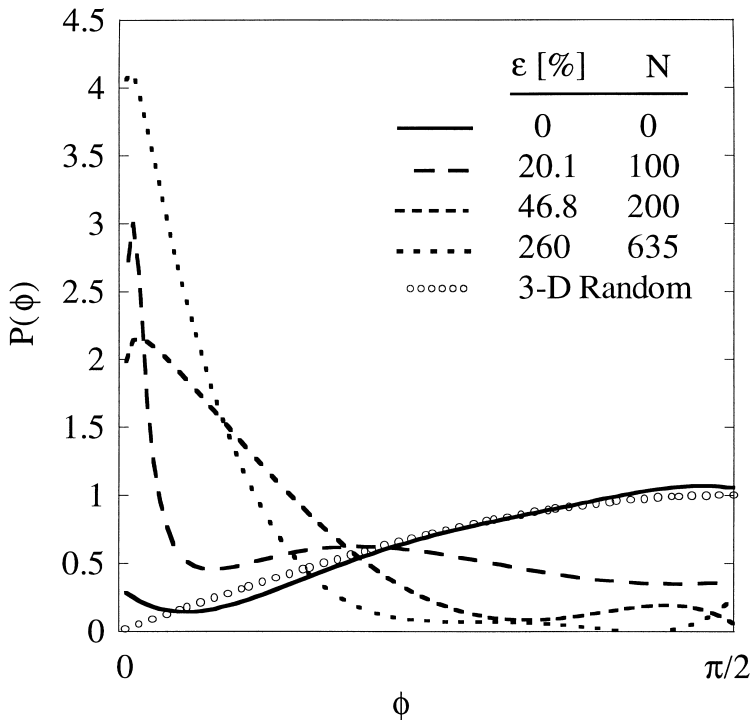Fig. 6. Probability density distributions for TiB whisker axial angles, ϕ, determined from electron back-scattering diffraction data. Distributions are shown for four specimens deformed to various engineering strains ϵ during N thermal cycles under 2.5 MPa applied tensile stress. The expected distribution for a three-dimensionally random array of whiskers (see the Appendix) is also shown.

Appendix, and shown for comparison in Fig. 6. The good agreement between this distribution and that of the TiB in the as-received composite indicates that the powder metallurgy production route results in a nearly random distribution of whiskers. Local fluctuations in some of the distributions in Fig. 6 may be due to the small sampling size, and could perhaps be removed by sampling over a larger number of whiskers.

During uniaxial deformation, only the whisker axial angle ϕ is affected by the matrix flow, while the random distribution of azimuthal whisker angles is unchanged. EBSD data identifying the TiB-[100], and [111] directions indeed confirmed that the distribution of whisker azimuthal angles showed no texture before or after deformation. Therefore, the microstructure remained transversely isotropic during all stages of the deformation. Finally, limited texture data of matrix α-grains was also acquired by the EBSD method, revealing no pronounced matrix texture either before or after deformation.

3.4. Room-temperature tensile properties of the superplastically deformed composite

Tabulated in Table 1 are the room-temperature 0.2% proof stress, ultimate tensile stress, and failure strain for two Ti–6Al–4V/TiB specimens tested in the as-received condition and after 100% engineering strain. A characteristically low tensile ductility of 0.3% was found for the former material (Saito et al., 1995). Despite the zero elongation to failure and the corresponding lack of a true proof or yield stress, the superplastically deformed specimen exhibited a small but significant increase in ultimate tensile strength of 11.2% compared with the as-received specimen.

4. Discussion

4.1. Stress dependence of transformation superplasticity

The stress dependence of $\Delta\varepsilon$ shown for the Ti–6Al–4V/TiB composite in Fig. 2 is in qualitative agreement with the linear relationship of the prevailing transformation superplasticity model by Greenwood and Johnson (1965), who predicted for a pure allotropic material:

$$\Delta\varepsilon \approx \frac{4}{3} \cdot \frac{5 \cdot n}{4 \cdot n + 1} \cdot \frac{\Delta V}{V} \cdot \frac{\sigma}{\sigma_0} \qquad (3)$$

for the case where transformation mismatch strain $\Delta V/V$ is accommodated by creep of the weakest phase with power-law stress exponent n, where the average internal stress generated during the transformation is σ_0 and the applied stress is small.

Upon the first demonstration of transformation superplasticity for a discontinuously-reinforced metal-matrix composite, Dunand and Bedell (1996) observed a marked increase in the superplastic slope $\Delta\varepsilon/\sigma$ for unalloyed titanium reinforced with 10 vol.% equiaxed TiC particulate (Ti/10 vol.% TiC) as compared

Table 1
Room temperature tensile properties of Ti–6Al–4V/TiB in the as-received ($\epsilon = 0\%$) and superplastically-deformed ($\epsilon = 100\%$) state, including 0.2% proof stress, $\sigma_{0.2\%}$, ultimate tensile strength, UTS, and elongation to failure, ϵ_f

ϵ (%)	$\sigma_{0.2\%}$ (MPa)	UTS (MPa)	ϵ_f (%)
0	804	856	0.3
100	$\geqslant 958$	958	0

to the unreinforced matrix. The present results display the opposite effect upon addition of discontinuous TiB whiskers to the alloy Ti–6Al–4V, a trend which is consistent with previous studies on other Ti–6Al–4V composites reinforced with 10 vol.% equiaxed TiC particulate rather than TiB whisker reinforcement. First, data of Zwigl and Dunand (unpublished work) for transformation superplasticity of Ti–6Al–4V and Ti–6Al–4V/10 vol.% TiC do not show the enhancement effect observed by Dunand and Bedell (1996). Second, Schuh et al. (1999) have recently studied the same two materials; their results on unreinforced Ti–6Al–4V are those shown in Fig. 2, and the superplastic slope they found for the Ti–6Al–4V/TiC composite was about 1.0 GPa^{-1}, the same value we find for Ti–6Al–4V/TiB with whisker reinforcement of the same fraction (Fig. 2). The quantitative match between the superplastic stress dependence of the TiC- and TiB-reinforced Ti–6Al–4V materials between these two studies is likely coincidental. Finally, a study of Ti–6Al–4V and Ti–6Al–4V/10 vol.% TiC under thermal cycling and biaxial bulging pressure was performed by Dunand and Myojin (1997), who observed significantly lower equivalent strains in the composite compared to the unreinforced alloy, despite identical deformation conditions and times. They attributed their result to a lower primary creep contribution to deformation for the composite, but the possibility of a lower steady-state contribution cannot be ruled out. In summary, all three of the existing studies of transformation superplasticity on alloyed Ti–6Al–4V and Ti–6Al–4V/10 vol.% TiC failed to reproduce the original enhancement observed by Dunand and Bedell (1996) for composites of commercial purity titanium, in agreement with the present result for Ti–6Al–4V/TiB composites.

A detailed examination of the cause of the decrease in superplastic slope upon reinforcement addition for alloyed Ti–6Al–4V is beyond the scope of the present article, and will be discussed in more detail in subsequent publications. However, an effect which is specific to the present TiB-composites is that load transfer to the whiskers may result in decreased matrix stresses, reducing the effective biasing stress on the transforming matrix and thereby decreasing $\Delta\varepsilon/\sigma$. We will examine this issue of load transfer in more detail in a later section.

4.2. Whisker alignment during deformation

4.2.1. Effect of matrix flow on alignment

The alignment of discontinuous fibers has previously been observed experimentally in Al/SiC metal-matrix composites subjected to superplastic elongational flows

induced by thermal expansion mismatch (Gonzalez-Doncel et al., 1989; Gonzalez-Doncel and Sherby, 1996). Whisker rotation has been modeled for conditions of extrusion, pure shear, and elongational flow, for both dilute and concentrated suspensions (Jeffery, 1923; Wu, 1979; Folgar and Tucker, 1984). The orientation of TiB observed in Figs. 5 and 6 is thus expected from both experimental and theoretical considerations. In all of the above cases, the reorientation of individual whiskers is due only to matrix flow. In our case, because of the very low solubility of B in the matrix (Anon., 1992), we expect that stress-directed diffusion plays only a small role in the reorientation of TiB (Fig. 6), which we attribute to superplastic flow of the matrix.

4.2.2. Effect of whisker alignment on superplastic deformation

During the course of superplastic deformation, the unreinforced Ti–6Al–4V alloy experienced only small relative variations in the strain increment $\Delta\varepsilon$ prior to the onset of failure [Fig. 4(a)]. Therefore, the considerable relative decrease in $\Delta\varepsilon/\sigma$ observed for the TiB-reinforced alloy [Fig. 4(b)] is likely an effect stemming from the presence of the reinforcing phase, and not from other microstructural changes, such as grain growth. We propose that this decrease and lack of steady-state deformation of the composite is associated with the evolution of the whisker orientation distribution, $P(\phi)$, as shown in Fig. 6. This hypothesis is examined in more detail below.

4.2.2.1. Elastic load transfer. The addition of whisker reinforcement to a metallic matrix deforming by a time-dependent mechanism such as creep or superplasticity often results in a decrease in deformation rate due to load sharing and flow constraints from the presence of reinforcement. A recent review of experimental and theoretical work on time-dependent deformation of such composites is given by Dunand and Derby (1993). Most theoretical models deal with the somewhat simplified cases of short fibers aligned in the flow direction (e.g. Kelly and Street, 1972) or continuous fibers (e.g. Yancey and Pindera, 1990; Chun and Daniel, 1997). In the present work, we are interested in the effect of the whisker axial angle distribution on the superplastic strain increment (i.e. average strain rate during cycling), for which there is presently no suitable model.

A rigorous description of creeping whisker-reinforced composites is beyond the scope of the present article. We instead examine the simpler case of elastic load transfer from the matrix to the reinforcing whiskers, and consider the effects of such load-sharing on the stress experienced by a matrix containing volume fraction f of reinforcing whiskers with axial angle distribution $P(\phi)$. The goal of this simplified approach is to justify the proposed correlation between the observed gradual whisker alignment [Fig. 6] and the decreasing superplastic strain increments observed for Ti–6Al–4V/TiB in Fig. 4(b).

During steady-state creep of discontinuously-reinforced composites, stress is partitioned between matrix and reinforcement according to the relative elastic moduli of the components (i.e. load transfer due to elastic strain mismatch) as well as the creep behavior of the matrix (i.e. load transfer due to plastic strain mismatch). The

use of elastic calculations to estimate the stress partitioning between phases therefore neglects plastic strain mismatch, which includes two significant effects (Clyne and Withers, 1993). First, plastic deformation of the matrix around an elastic particle increases strain mismatch between the phases, resulting in increased load transfer from matrix to whisker. Second, at high homologous temperatures, mismatch strains can be relaxed by stress driven (i.e. mismatch driven) diffusion or other relaxation processes. Neglecting the former effect results in overestimation of the stress borne by the matrix, while neglecting the latter effect has the opposite result. For a composite with large aspect-ratio reinforcement at high temperatures, diffusional relaxation can be expected to relieve some of the plastic strain mismatch — however, in general, both elastic and plastic strain mismatch still contribute to load transfer from matrix to reinforcement. The determination of the elastic contribution to load transfer therefore provides a lower bound on the whisker stress, or an upper bound on the matrix stress. For cases where relaxation processes are slow compared to the plastic deformation, more load is transferred to the whiskers, and elastic calculations quickly become inadequate. For the deformation of Ti–6Al–4V/TiB composites in the β-field of Ti–6Al–4V, the matrix self-diffusion is very rapid (Frost and Ashby, 1982), so we anticipate significant relaxation of plastic strain mismatch and therefore a significant contribution to load transfer from elastic strain mismatch. Examination of superplastically deformed composites (Fig. 5) shows no evidence of whisker fracture or of interfacial debonding, despite the extremely large plastic deformation of the matrix. This observation confirms that plastic strain mismatch is substantially relaxed during transformation superplasticity.

In the present case, where the matrix is deforming plastically while the reinforcing phase is elastic, load transfer from matrix to reinforcement affects creep through the reduction of the matrix stress. For unreinforced metals and alloys, the uniaxial creep rate, $\dot{\varepsilon}_1$, is governed by the three average principal stresses $\sigma_i(i = 1-3)$ according to a generalized creep equation (Finnie and Heller, 1959):

$$\dot{\varepsilon}_1 = A \cdot \sigma_{\text{eq}}^{n'-1} \cdot \left[\sigma_1 - \tfrac{1}{2}(\sigma_2 + \sigma_3) \right] \qquad (4)$$

where A is a constant, σ_{eq} is the von Mises equivalent stress, and n' is the creep stress exponent. As the above generalized creep equation applies for many materials and deformation mechanisms, it can be adapted to transformation superplasticity by (i) replacing the average strain rate $\dot{\varepsilon}_1$ with the superplastic strain increment $\Delta\varepsilon_1$, and (ii) introducing the stress exponent $n' = 1$, since $\Delta\varepsilon$ is proportional to σ [Eq. (3)]. For axisymmetric microstructure and specimen geometry we take $\sigma_2 = \sigma_3$. Finally, upon the addition of an elastic reinforcing phase, we describe the plastic deformation as being governed by the average matrix stresses, $< \sigma_i^{\text{M}} >$. This assumption alone is inadequate to describe the deformation, as constraint of matrix flow by the reinforcement further reduces the deformation rate. Use of $< \sigma_i^{\text{M}} >$ to describe the deformation thus requires the introduction of a geometric 'attenuation factor' which describes the fraction of the composite which flows under the average matrix stress.

For our purposes, we take this factor to be independent of $P(\phi)$ and combine it with the existing constants in Eq. (4) to form a new constant, C. Then Eq. (4) becomes:

$$\Delta\varepsilon_1 = C\cdot\left(\langle\sigma_1^M\rangle - \langle\sigma_2^M\rangle\right) \tag{5}$$

Predicting the effects of load transfer on deformation thus requires determining both the axial and transverse stresses in the matrix. We proceed by considering elastic load transfer to a whisker inclined at axial angle ϕ, summing the stress in each fiber given by the distribution $P(\phi)$, and finally extending to the case of a composite by the enforcement of mechanical equilibrium. The whiskers are taken as load-bearing only along their major axis, and elastic load transfer is calculated using the shear-lag model (Cox, 1952; Nardone and Prewo, 1986; Clyne, 1989; Clyne and Withers, 1993). Throughout the following sections superscripts of M, W, and C will correspond to the matrix, whisker(s), and composite, respectively.

We consider a unit cell as shown in Fig. 7, containing a single cylindrical whisker with axial angle ϕ with respect to the applied tensile stress. The coordinate system of the cell is differentiated from the global coordinate system with double-subscript notation, and the tensile axes for both systems are identical, $\sigma_1^C = \sigma_{11}^C$. In addition, a coordinate system aligned with the whisker axis is denoted by a prime.
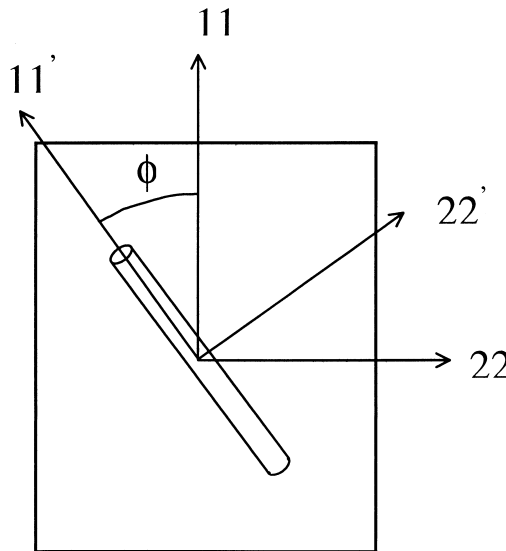

Fig. 7. Geometry of the ideal unit cell considered in the elastic load transfer calculations, with principal coordinate systems for the cell (11- and 22-axes) and aligned with the whisker at axial angle ϕ (11'- and 22'-axes). The 33- and 33'-axes are coincident and normal to the page, and the global 1-axis is coincident with the local 11-axis.

Elastic load transfer from matrix to whisker with aspect ratio s is described by the shear-lag model, which gives the average axial stress in a single whisker, $\sigma_{11}'^{W}$, as a function of applied tensile strain along the whisker axis:

$$\sigma_{11}'^{W} = E^{W} \cdot \varepsilon_{11}'^{C} \cdot \chi \tag{6}$$

where E is the Young's modulus, $\varepsilon_{11}'^{C}$ is the elastic strain of the unit cell in the $11'$-direction, and the constant χ is given by:

$$\chi = 1 - \frac{\tanh(m \cdot s)}{m \cdot s} \tag{7}$$

with

$$m = \left[\frac{2 \cdot E^{M}}{E^{W} \cdot (1 + \nu^{M}) \cdot \ln(1/f)} \right]^{\frac{1}{2}} \tag{8}$$

and the Poisson's ratio ν.

For elastic loading, we use Hooke's law for the unit cell, which in the coordinate system aligned with the whisker is written:

$$\varepsilon_{11}'^{C} = \frac{\sigma_{11}'^{C}}{E_{11}'^{C}} - \nu_{21}'^{C} \cdot \frac{\sigma_{22}'^{C}}{E_{22}'^{C}} \tag{9}$$

where the parameter ν_{ij} is Poisson's ratio corresponding to strains in the j direction upon application of stress in the i direction. The stresses in the 33- or 33'-direction are exactly zero, as there is neither applied stress nor load sharing in that direction. Following the initial assumption that the whisker only carries load along its major axis, we take $E_{22}'^{C} \approx E^{M}$. Furthermore, the Young's modulus of the composite along the direction of the whisker, $E_{11}'^{C}$, is given by the shear lag model and the application of mechanical equilibrium to the unit cell (Clyne and Withers, 1993):

$$E_{11}'^{C} = (1 - f) \cdot E^{M} + f \cdot \chi \cdot E^{W} \tag{10}$$

The Poisson's ratio $\nu_{21}'^{C}$ is more difficult to assign, but given that the elastic contractions in the $11'$ direction are governed primarily by the deformation of the whisker, we take $\nu_{21}'^{C} \approx \nu^{W}$ for cases where the whisker is much stiffer than the matrix. We note that the sensitivity of the results of these calculations to physically reasonable changes in $\nu_{21}'^{C}$ is small.

For the case of a uniaxial stress σ_{11}^{C} applied in the 11-direction, the average stresses $\sigma_{11}'^{C}$ and $\sigma_{22}'^{C}$ are related to the applied tensile stress by a rotational transformation about the 33-axis through the angle ϕ (Nye, 1985):

$$\sigma'^C_{11} = \sigma^C_{11} \cdot \frac{1}{2} \cdot (1 + \cos(2\phi)) = \sigma^C_{11} \cdot \cos^2\phi \tag{11a}$$

$$\sigma'^C_{22} = \sigma^C_{11} \cdot \frac{1}{2} \cdot (1 - \cos(2\phi)) = \sigma^C_{11} \cdot \sin^2\phi \tag{11b}$$

The rotation from principal axes to those aligned with the whisker results in shear components, e.g. σ'^C_{12}, which for the purposes of this analysis are neglected, and the load transfer from matrix to whisker is considered governed only by σ'^C_{11} according to the shear lag model [Eq. (6)]. Introduction of Eqs. (9) and (11) into Eq. (6) then gives the stress borne by the whisker:

$$\sigma'^W_{11} = E^W \cdot \chi \cdot \sigma^C_{11} \cdot \left(\frac{\cos^2\phi}{E'^C_{11}} - \nu^W \cdot \frac{\sin^2\phi}{E^M} \right) \tag{12}$$

This result is very similar in form to that presented by Klipfel et al. (1990) for axial stresses in an ellipsoid as determined by the Eshelby inclusion method. If appropriate materials parameters, such as those for the Ti–6Al–4V/TiB system are selected, Eq. (12) numerically matches Eq. (8) of Klipfel et al. (1990) almost exactly. Additionally, a similar approach to that described above is taken by Hong and coworkers (Hong and Chung, 1995, 1996; Ryu and Hong, 1999). However, these authors make different assumptions regarding the stress state in the whisker, and transform the global stress tensor to the axis of the whisker by a simple vector decomposition, producing $\sin\phi$ or $\cos\phi$ terms, rather than the $\sin^2\phi$ and $\cos^2\phi$ terms that appear in Eq. (12) due to tensor rotation.

The average axial whisker stress can also be described in the coordinate system aligned with the cell, rather than that aligned with the whisker, by means of a second rotation operation. It should be noted, however, that the principle axes of the whisker are different than those of the unit cell, so the appropriate transformation is:

$$\sigma^W_{11} = \sigma'^W_{11} \cdot \cos^2\phi = E^W \cdot \chi \cdot \sigma^C_{11} \cdot \left(\frac{\cos^4\phi}{E'^C_{11}} - \nu^W \cdot \frac{\sin^2(2\phi)}{4 \cdot E^M} \right) \tag{13a}$$

$$\sigma^W_{22} = \sigma'^W_{11} \cdot \sin^2\phi = E^W \cdot \chi \cdot \sigma^C_{11} \cdot \left(\frac{\sin^2(2\phi)}{4 \cdot E'^C_{11}} - \nu^W \cdot \frac{\sin^4\phi}{E^M} \right) \tag{13b}$$

The extension from the simple case of a single cell to a composite consisting of many adjacent unit cells requires a method of tessellation which provides realistic boundary conditions on each cell. This is a complex problem commonly encountered in finite-element modeling of discontinuously-reinforced composites (Christman et al., 1989). In our case, differing whisker alignments in neighboring cells leads to aperiodic and unpredictable boundary conditions. However, in the dilute limit ($f \rightarrow 0$), each cell can be treated independently of its neighbors, i.e. each cell is

subjected only to the externally-applied stress field. Furthermore, finite element calculations by Christman et al. (1989) on elastic–plastic deformation of rigid aligned-whisker-containing composites have shown that the use of periodic or traction-free boundary conditions on such unit cells yields similar global deformation behavior in the elastic regime. We then proceed by assuming that the system is sufficiently dilute that the effects of boundary conditions between neighboring cells are small, and extend the simple case of a unit cell in tension to a composite consisting of many cells by the enforcement of mechanical equilibrium:

$$\left\langle \sigma_1^M \right\rangle = (1 - f)^{-1} \cdot \left\{ \sigma_1^C - f \cdot \left\langle \sigma_{11}^W \right\rangle \right\} \tag{14a}$$

$$\left\langle \sigma_3^M \right\rangle = \left\langle \sigma_2^M \right\rangle = -(1 - f)^{-1} \cdot f \cdot \left\langle \sigma_{22}^W \right\rangle \tag{14b}$$

where $\left\langle \sigma_{ii}^W \right\rangle$ is the average stress in all whiskers and $\left\langle \sigma_i^M \right\rangle$ is the average matrix stress. By means of Eqs. (14), the average stress in each whisker in the local coordinate system is related to the average stress carried by the matrix and the applied stress σ_1^C in the global reference frame. Consistent with the condition of axisymmetry, Eq. (14b) requires the equality of the two global transverse stresses.

Finally, the average stress in all whiskers is found by summing the stress of each individual whisker in the distribution $P(\phi)$:

$$\left\langle \sigma_{ii}^W \right\rangle = \int_0^{\pi/2} P(\phi) \cdot \sigma_{ii}^W \cdot \mathrm{d}\phi \tag{15}$$

The average stress components in the matrix are now directly calculated by the use of Eqs. (13) and (15) in Eqs. (14) and the introduction of appropriate materials parameters. Given these average matrix stresses, the deformation rate is given by Eq. (4), or, for transformation superplasticity of a transversely isotropic composite, by Eq. (5). Although we presently apply these calculations to the case of transformation superplasticity, they could also be applied more reasonably to cases of purely elastic loading, such as fiber fracture during low-temperature deformation (Klipfel et al., 1990), provided that the assumption of low volume fraction, as well as the many assumptions involved in the shear lag model, are valid.

4.2.2.2. Load transfer in superplastically-deforming Ti–6Al–4V/TiB. In the following, we apply the above equations to the case of superplasticity of Ti–6Al–4V/TiB composites and determine the effect of the gradual whisker alignment on the superplastic strain increment. The elastic constants and other parameters employed are shown in Table 2. The lack of material property data of TiB in the literature has been noted by other authors (Fan et al., 1994), and a common practice is the substitution of properties for TiB$_2$, which is the approach taken here as well. We note that this is a source of error in the calculations, but also observe that the average matrix stresses determined by Eqs. (14) are insensitive to small variations in E^W and ν^W and thus we anticipate only small effects due to the inaccuracy associated with this assumption.

Eq. (15) is solved numerically for the four whisker angle distributions in Fig. 6, allowing determination of the average matrix stresses [Eq. (14)] at four points in the deformation history (Fig. 4). Although we have experimentally determined the orientation distribution $P(\phi)$, predictions from existing models of whisker alignment during matrix flow (e.g. Folgar and Tucker, 1984) could alternatively be used as input to Eq. (15).

The two average matrix stresses determined by Eqs. (14) are listed in Table 3 normalized by the applied stress σ_1^C. As expected, $<\sigma_1^M>$ is positive and decreases monotonically as the whiskers align and load transfer from matrix to whisker increases. However, the transverse matrix stress, $<\sigma_2^M>$, first decreases and then increases as the alignment progresses, due to an inflection in Eq. (13b). We also note that for all of the distributions $P(\phi)$ in Fig. 6, transverse load sharing is small compared to longitudinal load sharing. The negative values of $<\sigma_2^M>$ in Table 3 result from positive values of $<\sigma_2^W>$, which arise from an average state of axial tension in the aligning whiskers ($\sigma_{11}^{'W}$ positive).

The quantity $(<\sigma_1^M> - <\sigma_2^M>)/\sigma_1^C$, which governs the superplastic strain increment per Eq. (5) is plotted as a function of N in Fig. 8, with the individual points corresponding to the whisker orientation distributions in Fig. 6. We note that the largest changes in matrix stress occur in the early stages of superplastic deformation, corresponding to the considerable whisker alignment observed after only 46.8% engineering strain (Fig. 6). One anomaly resulting from the present simple approach is the large matrix stress in the as-received case ($N=0$), with random

Table 2

Materials parameters employed in determination of the matrix/whisker load transfer for Ti–6Al–4V (Anon., 1979) and TiB (Anon., 1987) at $\sim$900°C

	Ti–6Al–4V	TiB/TiB$_2$
E (GPa)	37[a]	430
ν	0.32	0.14
s		20
f		0.1

[a] Calculated using $E = 2(1+\nu)G$, where G is shear modulus of β-Ti from Frost and Ashby (1982).

Table 3

Calculated average matrix stresses $<\sigma_1^M>$ normalized by the applied uniaxial tensile stress σ_1^C for the four whisker orientation distributions in Fig. 6, and corresponding total engineering strain ϵ and number of cycles N

N	ϵ (%)	$<\sigma_1^M>/\sigma_1^C$	$<\sigma_2^M>/\sigma_1^C$
0	0	1.023	0.004
100	20.1	0.820	−0.025
200	46.8	0.714	−0.034
635	260	0.636	−0.024

whisker distribution (Fig. 6), for which the majority of the whiskers lie at large angles to the loading axis. Since we assumed that the whiskers cannot bear load along their minor axes, and since shearing of the whiskers is neglected in the above analysis, the full load borne by such whiskers is underestimated and the matrix stress inflated. However, as the whiskers align and the average angle ϕ decreases, the calculations become more exact.

In Fig. 9(b) the strain increment $\Delta\varepsilon$ is shown normalized by the deformation-controlling matrix stress quantity, ($<\sigma_1^M> - <\sigma_2^M>$), which has been interpolated between the four data points in Fig. 8. The original superplastic data, normalized by the true applied stress [Fig. 4(b)], are replotted in Fig. 9(a) for ease of comparison. The two plots, Fig. 9(a) and (b), then, respectively represent the strain increment history without and with elastic load transfer effects considered. The result of normalization by the average matrix stresses, rather than the applied tensile stress, is two-fold. First, the large gradual decrease in strain increment observed in Fig. 9(a) is no longer present, replaced instead by a prolonged steady-state regime. Second, the onset of tertiary deformation behavior occurs earlier, now accounting for almost a
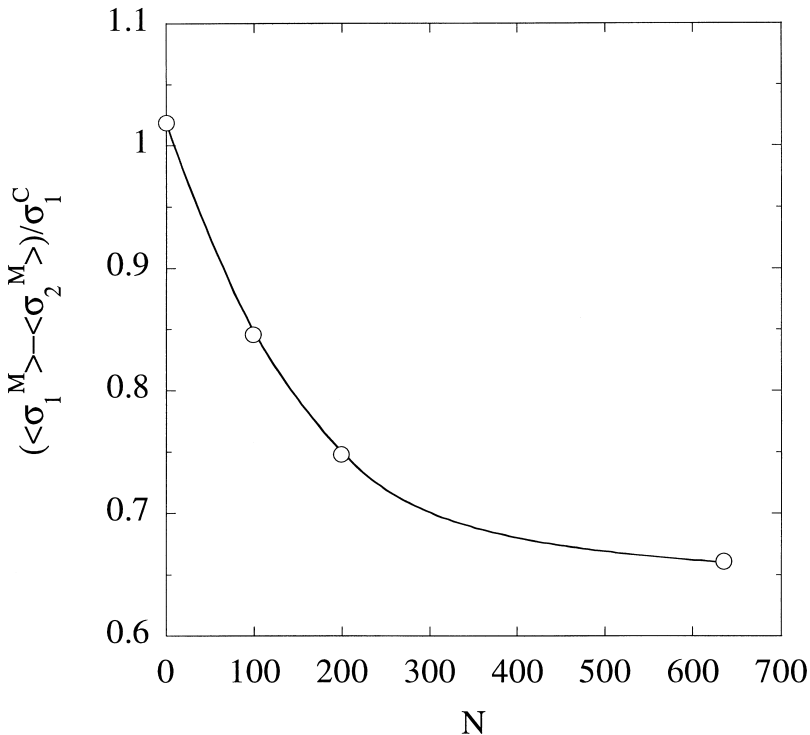

Fig. 8. Deformation-controlling average stress term from Eq. (5) plotted vs. the number of thermal cycles for the Ti–6Al–4V/TiB composite. Each point corresponds to a successively larger degree of orientation of the reinforcing whiskers (Fig. 6). Solid trend-line is found by interpolation.
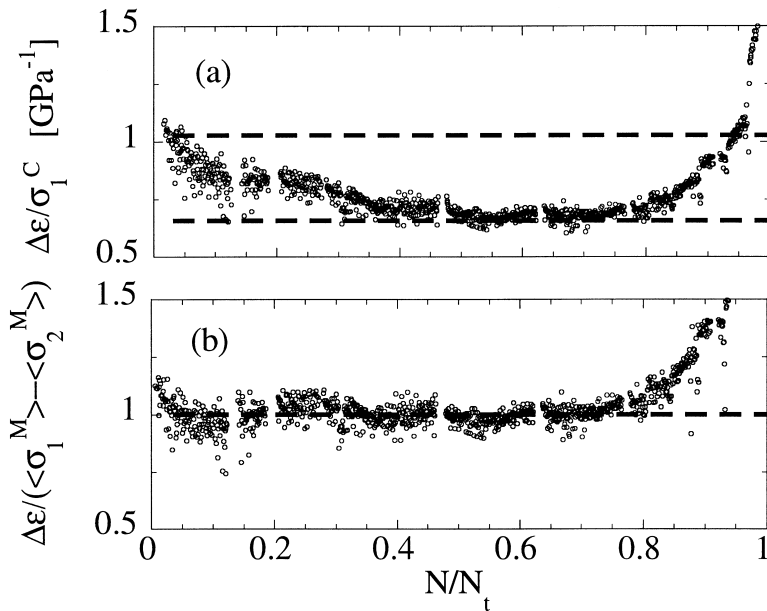
Fig. 9. Strain-increment history of Ti–6Al–4V/TiB normalized (a) by the applied true stress, as in Fig. 4, and (b) by the deformation-controlling matrix stresses as per Eq. (5). N/N_t is the specimen life-time fraction.

third of the specimen lifetime. Indeed, these changes result in a strain increment history which closely resembles that of the unreinforced Ti–6Al–4V material [Fig. 4(a)]. We conclude, therefore, that load transfer due to elastic strain mismatch between matrix and whiskers, and the gradual alignment of the whiskers, can explain the apparent strain-hardening observed during superplastic deformation for the Ti–6Al–4V/TiB composites. The lack of $\Delta\varepsilon$ dependence on N (for $N/N_t < 0.7$) in Fig. 9(b) may be somewhat fortuitous, considering the simplicity of the calculations and the many assumptions made.

Finally, we note that these calculations of elastic load transfer cannot explain why the superplastic strain increments in Fig. 9 are markedly below those exhibited by the unreinforced matrix [Figs. 2 and 4(a)]. However, as already discussed, Ti–6Al–4V/TiC composites containing equiaxed reinforcement display similar behavior, despite expectations of considerably less load-sharing than for a whisker-reinforced composite. We thus conclude that the effect of reinforcement on transformation superplasticity of Ti–6Al–4V is due to more than simply elastic load-transfer effects. Other important effects include the impact of reinforcement on the phase transformation kinetics and matrix strength, changes in reinforcement solubility during thermal cycling, and additional load transfer effects due to plastic strain mismatch, which has been neglected in the above analysis. Some discussion on these topics will be presented in future publications.

5. Conclusions

We have investigated the effects of 10 vol.% TiB whisker reinforcement on transformation superplasticity of Ti–6Al–4V, with the following notable results:

- By thermal cycling about the α/β phase transformation range of the matrix, we measured a superplastic tensile strain to failure of 260%. Combined with the result that the strain increment developed on each thermal cycle is proportional to the external tensile stress, this constitutes the first observation of transformation superplasticity of a whisker-reinforced metal matrix composite.
- Uniaxial superplastic flow resulted in gradual alignment of the whisker reinforcement, as commonly observed for shear flow or extrusion of composites. The degree of alignment was quantified by electron back-scattering diffraction, and is presented as an angular probability density distribution.
- Commensurate with gradual whisker alignment, a decrease in the superplastic strain rate and a lack of steady-state deformation behavior were observed. These effects can be justified by calculations which indicate that elastic strain-mismatch between matrix and whisker gradually increases during whisker alignment, leading to increased load transfer from matrix to whiskers.
- Room temperature tensile properties of the composites are not compromised by transformation superplastic straining. Instead, a small but significant increase in ultimate tensile strength was observed after superplastic deformation to 100% engineering strain.

Acknowledgements

Appendix

The EBSD texture analysis method samples local crystallographic orientation on a surface, not through the specimen volume, and therefore the probability of sectioning through individual whiskers with various axial angles must be considered. This problem is closely related to the so-called *Buffon Needle Problem*, described in, e.g. Russ (1986), where the probability of a dropped needle intersecting parallel grid lines on a sheet of paper is considered. In our case, TiB whiskers are analogous to the needles, and the cut surface used in EBSD analysis is analogous to a grid line in

two-dimensional space. For sectioning of the composites, the spacing of the 'grid lines' is very large compared to the whisker length. Noting that the tensile specimens were sectioned longitudinally, geometrical arguments show that the probability of a long whisker with axial angle ϕ intersecting the cut surface, $p(\text{int}|\phi)$, follows the proportionality:

$$p(\text{int}|\phi) \propto \sin\phi \qquad (\text{A1})$$

To recover the distribution $P(\phi)$ which is representative of a volumetric sampling, the experimentally-determined distribution of orientations on the cut surface are normalized by the above relationship, and subsequently scaled to satisfy the distribution normalization condition [Eq. (1)].

In a true three-dimensionally random distribution of whiskers, the probability of selecting a whisker with arbitrary axial and azimuthal angles in the ranges $[\phi, \phi + \delta\phi]$ and $[\theta, \theta + \delta\theta]$, respectively, is independent of those angles; each pair of angles is equally likely to occur. Correspondingly, the probability of randomly selecting a whisker exhibiting an axial angle in the range $[\phi, \phi + \delta\phi]$, independent of the azimuthal angle θ, is dependent upon ϕ itself. The geometry of the problem is shown in Fig. A1, and the probability $p(\phi)$ of a whisker exhibiting axial angle between ϕ and $\phi + \delta\phi$ is proportional to the area of a spherical surface swept out by the range $\phi + \delta\phi$. From simple geometry it can be shown that:

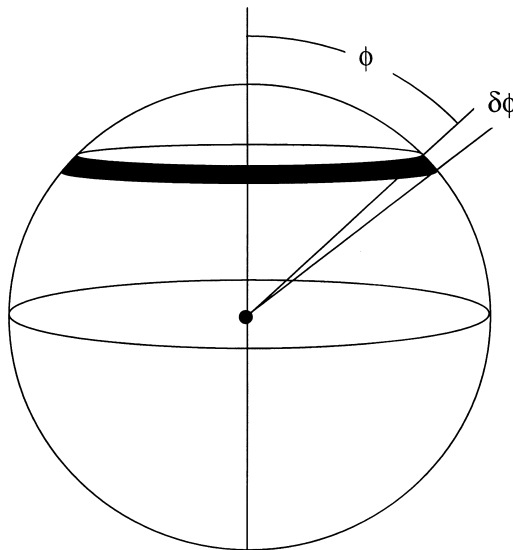$$p(\phi) \propto \sin\phi \qquad (\text{A2})$$

Fig. A1. Spherical geometry which describes all possible whisker orientations. For a three-dimensionally random arrangement of whiskers, the probability of randomly selecting a whisker with axial angle in the range $[\phi, \phi + \delta\phi]$ is proportional to the area of the shaded annulus.

A probability density can be obtained by normalization with the surface area of a sphere, resulting in the same proportionality. Thus, for a truly three-dimensionally random arrangement of whiskers the distribution of axial angles $P(\phi)$ is expected to increase in a sinusoidal fashion from 0 at $\phi = 0$ to a maximum at $\phi = \pi/2$.

References

Abkowitz, S., Weihrauch, P., 1989. Trimming the cost of MMCs. Adv. Mater. Proc. 136 (7), 31–34.

Abkowitz, S., Weihrauch, P.F., Abkowitz, S.M., 1993a. Particulate reinforced titanium alloy composites economically formed by combined cold and hot isostatic pressing. Industrial Heating 9, 32–37.

Abkowitz, S., Weihrauch, P., Abkowitz, S.M., 1993b. Advanced powder metal titanium alloy matrix composites reinforced with ceramic and intermetallic particles. In: Titanium Science and Technology '92. TMS, Warrendale, pp. 2511–2519.

Anon., 1979. Metals Handbook: Properties and Selection: Nonferrous Alloys and Pure Metals. ASM International, Metals Park, OH.

Anon., 1987. Engineered Materials Handbook, Vol. 4. Ceramics and Glasses. ASM International, Metals Park, OH.

Anon., 1992. ASM Handbook: Alloy Phase Diagrams. ASM International, Metals Park, OH.

Chaix, C., Lasalmonie, A., 1981. Transformation induced plasticity in titanium. Res. Mech. 2, 241–249.

Cherakaoui, M., Berveiller, M., Sabar, H., 1998. Micromechanical modeling of martensitic transformation induced plasticity (TRIP) in austenitic single crystals. Int. J. Plast. 14, 597–626.

Christman, T., Needleman, A., Nutt, S., Suresh, S., 1989. On microstructural evolution and micromechanical modeling of deformation of a whisker-reinforced metal matrix composite. Mater. Sci. Eng. A107, 49–61.

Chun, H.J., Daniel, I.M., 1997. Transverse creep behavior of a unidirectional metal matrix composite. Mech. Mater. 25, 37–46.

Clyne, T.W., 1989. A simple development of the shear lag theory appropriate for composites with a relatively small modulus mismatch. Mater. Sci. Eng. A122, 183–192.

Clyne, T.W., Withers, P.J., 1993. An Introduction to Metal Matrix Composites. Cambridge University Press, Cambridge pp. 20–27.

Cox, H.L., 1952. The elasticity and strength of paper and other fibrous materials. Brit. J. Appl. Phys. 3, 72–79.

Dunand, D.C., 1997. Transformation superplasticity in metals, alloys and composites. In: International Conference on Thermomechanical Processing of Steels and Other Materials. TMS, pp. 1821–1830.

Dunand, D.C., Bedell, C.M., 1996. Transformation-mismatch superplasticity in reinforced and unreinforced titanium. Acta Mater. 44, 1063–1076.

Dunand, D.C., Derby, B., 1993. Creep and thermal cycling. In: Suresh, S., Mortensen, A., Needleman, A. (Eds.), Fundamentals of Metal Matrix Composites. Butterworth-Heinemann, Boston, pp. 191–214.

Dunand, D.C., Myojin, S., 1997. Biaxial deformation of Ti–6Al–4V and Ti–6Al–4V/TiC composites by transformation-mismatch superplasticity. Mater. Sci. Eng. 230A, 25–32.

Fan, Z., Miodowinuk, P., Chandrasekaran, L., Ward-Close, M., 1994. The Young's moduli of in-situ Ti/TiB composites obtained by rapid solidification processing. J. Mater. Sci. 29, 1127–1134.

Farkash, M., Brandon, D.G., 1994. Whisker alignment by slip extrusion. Mater. Sci. Eng. A177, 269–275.

Finnie, I., Heller, W.R., 1959. Creep of Engineering Materials. McGraw Hill, New York.

Folgar, F., Tucker III, C.E., 1984. Orientation behavior of fibers in concentrated suspensions. J. Reinforced Plastics and Composites 3, 98–119.

Frost, H.J., Ashby, M.F., 1982. Deformation-Mechanism Maps: The Plasticity and Creep of Metals and Ceramics. Pergamon Press, Oxford pp. 43–52.

Funami, K., Kobayashi, M., Suzuki, S. and Ouchi, C. (1997). Superplasticity of fine TiB dispersed Ti–6Al–4V alloy composites obtained by reaction sintering. Mater. Sci. Forum, 243–245, 515–520.

Gonzalez-Doncel, G., Karmarkar, S.D., Divecha, A.P., Sherby, O.D., 1989. Influence of anisotropic distribution of whiskers on the superplastic behavior of aluminum in a back extruded 6061 Al–20% SiC$_w$ composite. Comp. Sci. Technol. 35, 105–120.

Gonzalez-Doncel, G., Sherby, O.D., 1996. Tensile ductility and fracture of superplastic aluminum SiC composites under thermal cycling conditions. Metall. Mater. Trans. 27A, 2837–2842.

Gorsse, S., Chaminade, J.P., Petitcorps, Y.L., 1998. In situ preparation of titanium base composites reinforced by TiB single crystals using a powder metallurgy technique. Composites 29A, 1229–1234.

Greenwood, G.W., Johnson, R.H., 1965. The deformation of metals under small stresses during phase transformations. Proc. Roy. Soc. Lond. 283A, 403–422.

Hong, S.H., Chung, K.H., 1995. High temperature creep behavior of SiC/2124Al metal matrix composites. Key Engineering Materials 104–107, 757–764.

Hong, S.H., Chung, K.H., 1996. Phenomena and mechanism of high-temperature creep of SiC/2124Al metal matrix composites. In: Arsenault, R.J. et al. (Ed.), The Johannes Weertman Symposium. TMS, Warrendale, PA, pp. 61–67.

Hyman, M.E., McCullough, C., Valencia, J.J., Levi, C.G., Mehrabian, R., 1989. Microstructure evolution in TiAl alloys with B additions: conventional solidification. Metall. Trans. 20A, 1847–1859.

Jeffery, G.B., 1923. The motion of ellipsoidal particles immersed in a viscous fluid. Proc. Roy. Soc. Lond. A102, 161–179.

Kelly, A., Street, K.N., 1972. Creep of discontinuous fibre composites. II. Theory for the steady state. Proc. Roy. Soc. Lond. A328, 283–293.

Klipfel, Y.L., He, M.Y., McMeeking, R.M., Evans, A.G., Mehrabian, R., 1990. The processing and mechanical behavior of an aluminum matrix composite reinforced with short fibers. Acta Metall. Mater. 38, 1063–1074.

Leblond, J.B., 1989. Mathematical modelling of transformation plasticity in steels. II: Coupling with strain hardening phenomena. Int. J. Plast. 5, 573–591.

Leblond, J.B., Devaux, J., Devaux, J.C., 1989. Mathematical modelling of transformation plasticity in steels. I: Case of ideal plastic phases. Int. J. Plast. 5, 551–572.

Lederich, R.J., Soboyejo, W.O., Srivatsan, T.S., 1994. Preparing damage-tolerant titanium-matrix composites. JOM 11, 68–71.

Li, D.X., Ping, D.H., Lu, Y.X., Ye, H.Q., 1993. Characterization of the microstructure in TiB-whisker reinforced Ti alloy matrix composite. Mater. Let. 16, 322–326.

Nardone, V.C., Prewo, K.M., 1986. On the strength of discontinuous silicon carbide reinforced aluminum composites. Scripta Metall. 20, 43–48.

Nye, J.F., 1985. Physical Properties of Crystals. Oxford Press, Oxford 43–46.

Ranganath, S., 1997. A review on particulate-reinforced titanium matrix composites. J. Mater. Sci. 32, 1–16.

Russ, J.C., 1986. Practical Stereology. Plenum Press, New York pp. 165–166.

Ryu, H.J., Hong, S.H., 1999. Analysis of load transfer and high temperature creep behavior of SiC$_W$/Al metal matrix composites. In: Mishra, R.S., Mukherjee, A.K., Murty, K.L. (Eds.), Creep Behavior of Advanced Materials for the 21st Century. TMS, Warrendale, PA, pp. 159–170.

Saito, T. (1995). A cost-effective P/M titanium matrix composite. Advanced Performance Materials, 2, 121-144

Saito, T., Furuta, T., Yamaguchi, T., 1994. A low cost titanium alloy composite. In: Metallurgy and Technology of Practical Titanium Alloys. TMS, Warvendale, PA, pp. 351–362.

Saito, T., Furuta, T., Yamaguchi, T., 1995. Development of low cost titanium matrix composite. In: Recent Advances in Titanium Metal Matrix Composites. TMS, Warvendale, PA, pp. 33–44.

Sato, K., Nishimura, T., Kimura, Y., 1994. The temperature and the grains of Ti–6Al–4V alloy on the uniaxial and biaxial deformation for superplasticity. Mater. Sci. Forum 170-172, 207–212.

Schuh, C., Zimmer, W., Dunand, D.C., 1999. Microstructure and properties of titanium and Ti–6Al–4V with and without TiC$_P$ reinforcement deformed by transformation superplasticity. In: Mishra, R.S., Mukherjee, A.K., Murty, K.L. (Eds.), Creep Behavior of Advanced Materials for the 21st Century. TMS, Warrendale PA, pp. 61–70.

Takayama, Y., Furushiro, N., Hori, S., 1985. Transformation superplasticity in a commercial pure titanium. In: Titanium Science and Technology. Deutsche Gesellschaft fur Metallkunde, Munich, pp. 753–760.

Wu, S., 1979. Order-disorder transitions in the extrusion of fiber-filled poly (ethylene terephthalate) and blends. Polym. Eng. Sci. 19, 638–650.

Yamamoto, T., Otsuki, A., Ishihara, K., Shingu, P.H., 1997. Synthesis of near net shape high density TiB/Ti composite. Mater. Sci. Eng. A239-240, 647–651.

Yancey, R.N., Pindera, M.J., 1990. Micromechanical analysis of the creep response of unidirectional composites. J. Eng. Mater. Technol. 112, 157–163.

Zwigl, P., Dunand, D.C., 1998. Transformation superplasticity of zirconium. Metall. Mater. Trans. 29A, 2571–2581.